



Clusters and their fundamental role for Trojan Horse Method

R. G. Pizzone^{1,a}, C. A. Bertulani², L. Lamia^{1,3,4}, M. La Cognata¹, M. L. Sergi^{1,3}, R. Spartá^{1,3}, A. Tumino^{1,5}

¹ Laboratori Nazionali del Sud-INFN, Catania, Italy

² Department of Physics and Astronomy, Texas A&M University-Commerce, Commerce, TX 75429, USA

³ Dipartimento di Fisica e Astronomia “Ettore Majorana”, Università di Catania, Catania, Italy

⁴ CSFNSM-Centro Siciliano di Fisica Nucleare e Struttura della Materia, Catania, Italy

⁵ Facoltà di Ingegneria e Architettura, Università degli Studi di Enna Kore, Enna, Italy

Received: 16 September 2020 / Accepted: 13 October 2020

© Società Italiana di Fisica and Springer-Verlag GmbH Germany, part of Springer Nature 2020

Communicated by Nicolas Alamanos

Abstract The Trojan Horse Method (THM) lays its foundations on the cluster structure of light nuclei which are usually used as “Trojan horses”. Many of them were successfully employed in the last decades to shed light to numerous astrophysical problems. Cluster structure and dynamics also suggest a series of tests which may be performed in order to strengthen the basis of the method. Among them pole invariance was investigated for three different situations. In fact, the cross sections for the ${}^6\text{Li}(d, \alpha){}^4\text{He}$, ${}^2\text{H}(d, p){}^3\text{H}$ and ${}^7\text{Li}(p, \alpha){}^4\text{He}$ binary reactions were measured for several break-up schemes and analyzed within the framework of the Plane Wave Impulse Approximation (PWIA). The indirect results extracted by using different Trojan Horse nuclei (e.g. ${}^2\text{H}$, ${}^3\text{He}$, ${}^6\text{Li}$) were compared with each other as well as with direct measurements of the corresponding astrophysical reactions. The very good agreement obtained confirms the applicability of the pole approximation and of the pole invariance method, namely the independence of binary indirect cross section on the chosen Trojan Horse nucleus, at least for the cases investigated. Moreover, we can verify that the effect of using a charged or a neutral particle as a spectator implies negligible corrections consistent with the experimental errors. In addition, the dynamics of clusters inside the Trojan Horse nucleus and their fingerprints on the measured momentum distribution play a key role for THM applications. In this article we will therefore discuss also these assertions studied in different systems (${}^2\text{H}$, ${}^3\text{He}$, ${}^6\text{Li}$, ${}^9\text{Be}$, ${}^{14}\text{N}$) and in particular for the deuteron case the relative impact of s and d waves in the momentum distribution will also be examined.

1 Introduction

The study of nuclear processes induced by charged particles at astrophysical energies has many experimental difficulties, mainly connected to the presence of the Coulomb barrier and the electron screening effect. For these reasons several indirect methods have been developed in the last 30 years, mainly based on direct reactions. Among them, an important role is played by the Trojan Horse Method (THM) [1, 2]. It has been applied to numerous reactions in the past decades [3–7] at the energies relevant for astrophysical applications, which usually are far below the Coulomb barrier. In recent years many tests have been made to deepen the knowledge of the method and extend its possible applications to neutron capture reactions on stable nuclei using neutron beams [8–10], or radioactive ion beams [11–13], and even to the interaction of neutrons and unstable nuclei [14, 15].

THM allows the extraction of the low energy behaviour of a binary reaction cross section relevant for astrophysics by applying the Quasi-Free (QF) reaction formalism. QF processes are direct mechanisms in which the interaction between an impinging nucleus and the target can cause the break-up of the target (TBU) or of the projectile (PBU). In particular, these processes have three particles in the exit channel, one of which can be thought as a spectator for the binary interaction of interest. In case of TBU, the assumption is that of an interaction between the impinging nucleus a and one of the clusters constituting the target (called participant, x , with $b = x + s$), while the residual nucleus, s , does not participate in the reaction. The fact that s is a spectator is reflected in the exit channel by displaying the same momentum distribution as for the inter-cluster (xs) motion inside b it had before the occurrence of the QF break-up.

In most applications the simplest Trojan Horse (TH) nucleus, i.e., deuterium was used. This allows the possibil-

^a e-mail: rgpizzone@lns.infn.it (corresponding author)

Table 1 Trojan Horse nuclei employed during the last decades of THM applications. Possible virtual beams which can be extracted from them are listed in second column

| TH nucleus | Virtual beam | Refs. |
|-------------------|---------------------------|-------|
| ${}^2\text{H}$ | p,n | [17] |
| ${}^6\text{Li}$ | α, d | [18] |
| ${}^3\text{He}$ | p,d | [19] |
| ${}^9\text{Be}$ | $\alpha, {}^5\text{He}$ | [20] |
| ${}^{14}\text{N}$ | ${}^{12}\text{C}, \alpha$ | [16] |

ity to deploy n or p participants as virtual beams. After that several nuclides were used for the same purpose. One of the most employed TH particles is ${}^6\text{Li}$, which can be modeled as $\alpha \oplus d$, thus extending the possible participants to be used for THM applications. As reported in Table 1, ${}^3\text{He}$ and ${}^9\text{Be}$ were also used in many applications. In the very recent past and in order to study reactions involving heavier nuclides (e.g. the ${}^{12}\text{C} + {}^{12}\text{C}$ reaction [16]), different TH nuclei were used such as ${}^{14}\text{N}$, ${}^{16}\text{O}$. In future applications also ${}^{20}\text{Ne}$ will be tested as a possible source of alphas and ${}^{16}\text{O}$.

A derivation of the PWIA cross section for the process $a(b, cC)s$ in the pole approximation, according to the Butler theory [21–23], is given in reference [19] and references therein. There, it is shown that the three-body cross section for the process of interest is given by

$$\sigma(\theta, \phi) \simeq \frac{\mu_i \mu_f P_f}{(2\pi)^2 P_i} |\varphi_{sx}(\mathbf{q}_s)|^2 |\mathcal{V}_{cC}(\mathbf{q}_C)|^2,$$

where i (f) denote the initial (final) channel, μ is the reduced mass, P is the center of mass momentum and \mathbf{q} is the momentum transfer. φ_{sx} is the momentum transform of the relative motion wave function for the $s + x$ two-body system.

Except for phase space factors, the momentum transform $\mathcal{V}_{cC}(\mathbf{q}_C)$ in Eq. 1 is nothing more than the scattering amplitude for the $c + C$ system when $\phi_{cC}(\mathbf{r}_{cC})$ is taken as a scattering wave. Equation 1 is thus proportional to the (off-shell) reaction scattering cross section $d\sigma/d\Omega$ for the two body $a(x, c)C$ reaction. Notice that the derivation of Eq. 1 and its factorization into two separate terms makes it evident that there is no dependence on the Trojan horse nucleus b if the final channel includes the same set of $c + C$ particles. Hence, except for changes in the kinematical factor KF , the cross sections for the $a(x, cC)$ extracted from the $a(b, cC)s$ reaction is completely (if all approximations are valid) equivalent to that extracted from the $a(b', cC)s'$ reaction. We call this the *pole invariance*.

In this framework this important test, has been performed. It means, in simple words, that the study of a binary reaction of astrophysical interest, $a(x, c)C$, via a QF process with three particles in the exit channel, can proceed whatever the spectator particle is. It means that instead of studying the

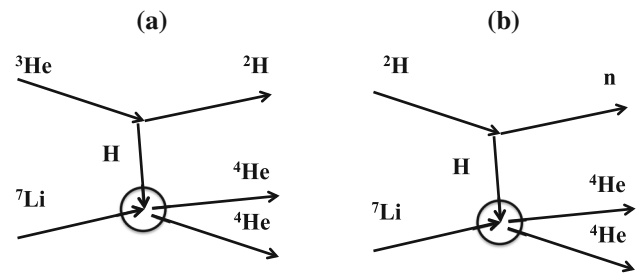


Fig. 1 Left: Pole diagram describing the quasi-free mechanism in the case of ${}^3\text{He}$ -breakup. Right: Pole diagram describing the quasi-free mechanism in the case of ${}^2\text{H}$ -breakup for the ${}^7\text{Li}(p, \alpha){}^4\text{He}$ reaction

binary reaction through the $a(b, cC)s$ reaction, one can study it by means of the $a(b', cC)s'$ reaction. This is clearer if we think about a practical case as it is sketched in Fig. 1 for the ${}^7\text{Li}(p, \alpha){}^4\text{He}$ binary reaction studied either ${}^3\text{He}$ break-up (charged spectator deuteron, panel a) or d break-up (neutron spectator, panel b). This represents the invariance of the lower vertex of the polar diagram with respect to changes in the upper one (break-up of Trojan horse nucleus).

A particular and important case is when a comparison can be done between a charged spectator and a neutral one. An eventual invariance of THM results despite the electrical charge of the spectator particle clearly shows that within the experimental errors a charged spectator does not introduce relevant distortions to the study of the reaction of interest (upper vertex).

Based on the discussion above, we can factorize the $a(b, cC)s$ three body cross section into two terms [18],

$$\frac{d^3\sigma}{dE_c d\Omega_c d\Omega_C} \propto KF \left(\frac{d\sigma}{d\Omega_{cm}} \right)^{HOES} \cdot |\varphi(\mathbf{p}_s)|^2, \quad (1)$$

where

- $[(d\sigma/d\Omega)_{cm}]^{HOES}$ is the half-off-energy-shell (HOES) differential cross section for the two body $a(x, c)C$ reaction at the relative $a-x$ energy E_{ax} given in post-collision prescription by

$$E_{ax} = E_{cC} - Q_{2b}, \quad (2)$$

Q_{2b} is the two body Q-value of the $a + x \rightarrow c + C$ reaction and E_{cC} is the relative energy between the outgoing particles c and C ;

- KF is a kinematical factor containing the final state phase-space factor and it is a function of the masses, momenta and angles of the particles [18];
- $\varphi(\mathbf{p}_s) \equiv \varphi_{sx}(\mathbf{q}_s)$ is the Fourier transform of the $a = (sx)$ bound state wave function $\phi_{sx}(\mathbf{r}_{sx})$.

If $|\varphi(\mathbf{p}_s)|^2$ is known and KF is calculated, it is possible to derive $[(d\sigma/d\Omega)_{cm}]^{HOES}$ from a measurement of

Table 2 Physical cases for which the Trojan Horse particle invariance was investigated. The relevant reference for each reaction is reported in the last column

| Quasi-free process | Binary reaction | TH particle | Ref. |
|--|---------------------------------|-----------------|---------|
| ${}^6\text{Li}({}^6\text{Li},\alpha\alpha){}^4\text{He}$ | ${}^6\text{Li}(d,\alpha)\alpha$ | ${}^6\text{Li}$ | [19] |
| ${}^6\text{Li}({}^3\text{He},\alpha\alpha)\text{H}$ | ${}^6\text{Li}(d,\alpha)\alpha$ | ${}^3\text{He}$ | [19] |
| ${}^7\text{Li}(d,\alpha\alpha)\text{n}$ | ${}^7\text{Li}(p,\alpha)\alpha$ | d | [19,30] |
| ${}^7\text{Li}({}^3\text{He},\alpha\alpha){}^2\text{H}$ | ${}^7\text{Li}(p,\alpha)\alpha$ | ${}^3\text{He}$ | [19,30] |
| ${}^2\text{H}({}^6\text{Li},\text{pt}){}^4\text{He}$ | $d(d,p)t$ | ${}^6\text{Li}$ | [31] |
| ${}^2\text{H}({}^3\text{He},\text{pt})\text{H}$ | $d(d,p)t$ | ${}^3\text{He}$ | [31] |

$d^3\sigma/dE_c d\Omega_c d\Omega_C$ by using Eq. 1.

$$\left(\frac{d\sigma}{d\Omega}\right)^{HOES} \propto \left[\frac{d^3\sigma}{dE_c d\Omega_c d\Omega_C}\right] \cdot [KF|\varphi(\mathbf{p}_s)|^2]^{-1}. \quad (3)$$

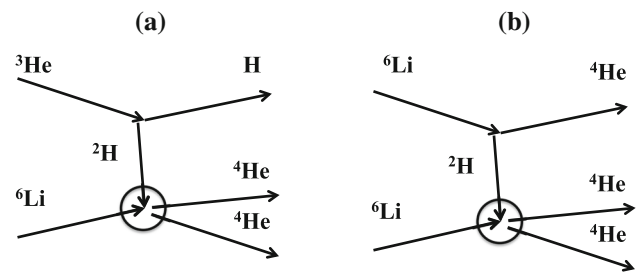
In the experimental analysis the validity conditions of the PWIA have to be fulfilled. In the THM we are interested in obtaining the energy trend of the HOES binary reaction cross section $[(d\sigma/d\Omega)_{cm}]^{HOES}$ rather than in its absolute value. The latter can be extracted through normalization to the direct data available at higher energies. Extensive reviews on the method are available in [24–27].

The success of THM relies on the quasi-free kinematics ($p_s \sim 0$ for target Trojan Horse nuclei, the most used being ${}^3\text{He}$, ${}^6\text{Li}$ or ${}^2\text{H}$), at which the TH conditions are best fulfilled. It has also been verified that for spectator momenta around zero the PWIA gives results similar to those obtained by more complicate approaches, as reported in Ref. [28].

The present paper will be devoted to the investigation of the role of cluster and their dynamics in THM principles and applications. In particular we will examine pole invariance tests for the THM in several experimental cases such as the ${}^7\text{Li}(p,\alpha){}^4\text{He}$ reaction, ${}^6\text{Li}(d,\alpha){}^4\text{He}$ case and the ${}^2\text{H}(d,p){}^3\text{H}$ (see Table 2). Such studies are crucial, as THM has become one of the major tools for the investigation of reactions of astrophysical interest using indirect methods and radioactive beam facilities (for a recent review see, e.g. [29]). After we will review the specific role of cluster motion in TH nuclei and in particular their momentum distribution, its importance for the foundations of THM and the bulk of information which can be achieved through it, as well as its impact on THM results.

2 Experimental results: ${}^6\text{Li}(d,\alpha){}^4\text{He}$ studied via ${}^6\text{Li}$ and ${}^3\text{He}$ break-up

The first case of a binary reaction to be studied according to QF break-ups arising from two different TH particles is the ${}^6\text{Li}(d,\alpha){}^4\text{He}$ reaction. This reaction was one of the first studied for a better understanding of the electron screen-

**Fig. 2** Study of ${}^6\text{Li}(d,\alpha){}^4\text{He}$ via THM. Left: Pole diagram describing the quasi-free mechanism in the case of ${}^3\text{He}$ -breakup. Right: Pole diagram describing the quasi-free mechanism in the case of ${}^6\text{Li}$ -breakup

ing phenomenon by THM via ${}^6\text{Li}$ break-up ([18]). Successfully a full investigation of the same reactions was performed by means of the ${}^6\text{Li}({}^3\text{He},\alpha\alpha)\text{H}$ process (see Fig. 2 for different break-up schemes). These latter data together with the comparison of the results with those arising from ${}^6\text{Li}({}^6\text{Li},\alpha\alpha){}^4\text{He}$ reaction are presented in [19]. The quasi-free contribution is extracted and the THM applied to retrieve information on the pole invariance of the ${}^6\text{Li}(d,\alpha){}^4\text{He}$ cross section at energies above and below the Coulomb barrier for both QF reactions. A good agreement with the direct data is achieved in the whole explored energy range thus allowing normalization. If we zoom in Fig. 3 in the energy range 0.4–1 MeV, we can compare data for the ${}^6\text{Li}(d,\alpha){}^4\text{He}$ arising from the ${}^6\text{Li}({}^3\text{He},\alpha\alpha)\text{H}$ reaction with the ones extracted from ${}^6\text{Li}({}^6\text{Li},\alpha\alpha){}^4\text{He}$ [18]. The agreement is very good within the experimental errors. This confirms the assumption that changing the spectator particle in the quasi-free process (on which is founded the THM) does not give any change to the binary reaction of interest. Moreover in this case we can see no relevant difference between data with $Z = 2$ spectator (α from ${}^6\text{Li}$ break-up, blue circles) and with $Z = 1$ spectator (p from ${}^3\text{He}$ break-up). This shows that distortions arising from increased spectator charge are negligible within the experimental errors.

3 Experimental results: ${}^7\text{Li}(p,\alpha){}^4\text{He}$ studied via ${}^2\text{H}$ and ${}^3\text{He}$ break-up

The second case which was thoroughly investigated is the ${}^7\text{Li}(p,\alpha){}^4\text{He}$ reaction, a process which is crucial in several astrophysical scenarios like primordial nucleosynthesis [32] or light elements depletion [33–35]. Historically the first studies were performed by means of d break-up (see Refs. [17,36,37]). Following the same path discussed above it was decided to use an alternate break-up scheme (i.e. ${}^3\text{He}$ break-up, see Fig. 1) and thus test the pole approximation once again. In Ref. [36] the ${}^7\text{Li}(p,\alpha){}^4\text{He}$ was studied through the deuteron break-up while in [30] ${}^3\text{He}$ break-up was investi-

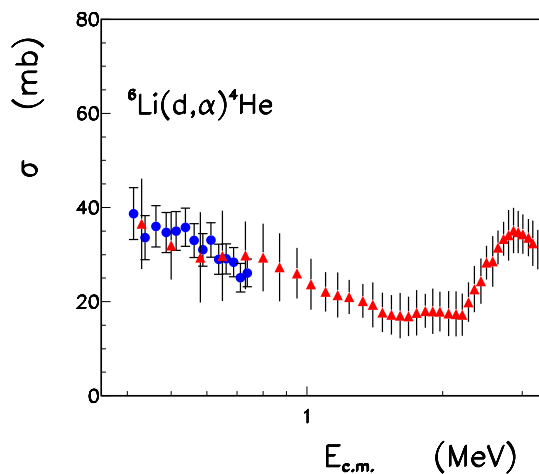


Fig. 3 Excitation function for the ${}^6\text{Li}(d,\alpha){}^4\text{He}$ reaction extracted by means of THM. The data from ${}^3\text{He}$ break-up (red triangles) are compared with the ones extracted from the ${}^6\text{Li}$ break-up (blue circles, [18]). The pole invariance test is clearly fulfilled

gated. In both cases resonances were clearly reproduced in the whole energy range.

The data extracted through d break-up from [36] are shown in Fig. 4 as empty circles superimposed onto the red dots from ${}^3\text{He}$ break-up. We can see that both resonances are reproduced and the agreement within the whole excitation function is very good also in this case. This gives a further validity test of the pole approximation in a different case and simultaneously above and below the Coulomb barrier. Also at lower energies the behaviour is coherent with data extracted from d break-up as reported in [17].

We want to stress that in this case results arising from a QF process with a neutral particle as a spectator are in very good agreement within experimental errors with those having a charged spectator (d in the present case). Consequently, with our present experimental limits it seems that the presence of a charged/neutral spectator does not affect the cross section measurement of the reactions of astrophysical interest.

4 Experimental results: ${}^2\text{H}(d,p){}^3\text{H}$ studied via ${}^6\text{Li}$ and ${}^3\text{He}$ break-up

The $d(d,p)t$ reaction has been tackled in two TH experiments, the first proceeding through ${}^6\text{Li}$ QF break-up, the second through ${}^3\text{He}$. Their schemes are depicted in Fig. 5.

The resulting astrophysical factors comes from analysis of two experiments described in details in [31,38] for the ${}^2\text{H}({}^6\text{Li}, pt){}^4\text{He}$ measurement and in [39] for the ${}^2\text{H}({}^3\text{He}, pt)\text{H}$. To proceed to the QF mechanism data extraction, the momentum distributions were treated as prescribed in [40]. For the ${}^6\text{Li}$ break-up distributions have been fitted with an Hänckel function (which turns out to be the most suit-

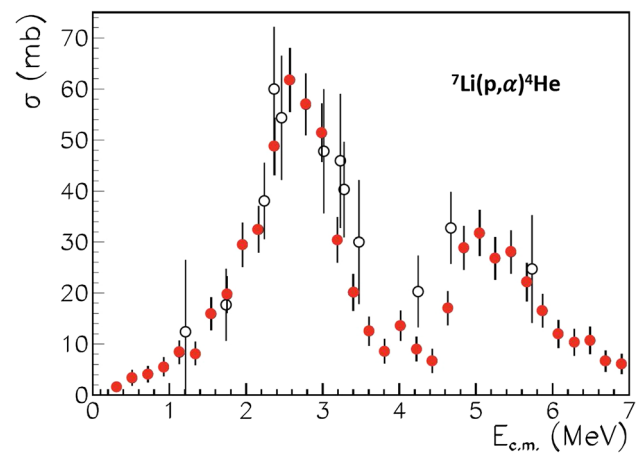


Fig. 4 Experimental ${}^7\text{Li}(p,\alpha){}^4\text{He}$ excitation function extracted by means of the THM using ${}^3\text{He}$ (red dots) and deuteron (open circles [36]) as Trojan Horse nucleus

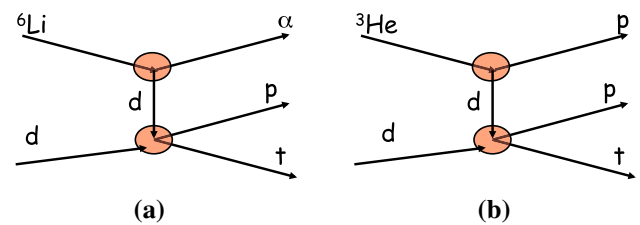


Fig. 5 QF break-up for $d(d,p)t$ sketches. Left **a**: the quasi-free reaction involving the ${}^6\text{Li}$ break-up is shown. Right **b**: the ${}^3\text{He}$ break-up is reported

able [41]), while an Eckart function has been used for the ${}^3\text{He}$ case. The binary cross section is extracted from the measured three-body one, for both cases, in order to extract the energy trend of the $S(E)$ -factors. Thus, the standard prescriptions of the THM were applied, as discussed in [27].

Results are shown in Fig. 6 where ${}^6\text{Li}$ break-up data are shown as green circles (see [31]) and the ones from ${}^3\text{He}$ break-up are the black triangles (see [39]). Errors bars shown in this figure include the normalization procedure and the errors connected to the penetrability factor. Here is evident how ${}^6\text{Li}$ break-up case lead to much larger errors, mainly because of the presence of the sequential mechanism in ${}^7\text{Li}$ (discussed in [38]) which decreased the QF events. These two experiments lead to S_0 values in agreement within the experimental errors, namely $S_0 = 75 \pm 21 \text{ keV}\cdot\text{b}$ (${}^6\text{Li}$ break-up) and $S_0 = 58 \pm 2 \text{ keV}\cdot\text{b}$ (${}^3\text{He}$ case), obtained with polynomial fits on the $S(E)$ data. These values are also in agreement with previous direct measurements [42,43]. Moreover, the use of these two different TH nuclei has lead to coherent results also for the electron screening potential extracted.

As for the case of Sect. 2, $Z = 2$ and $Z = 1$ spectators lead to no relevant difference between data, confirming that the spectator charge distortions are negligible within the experimental errors. Then, also in this case, we can conclude that

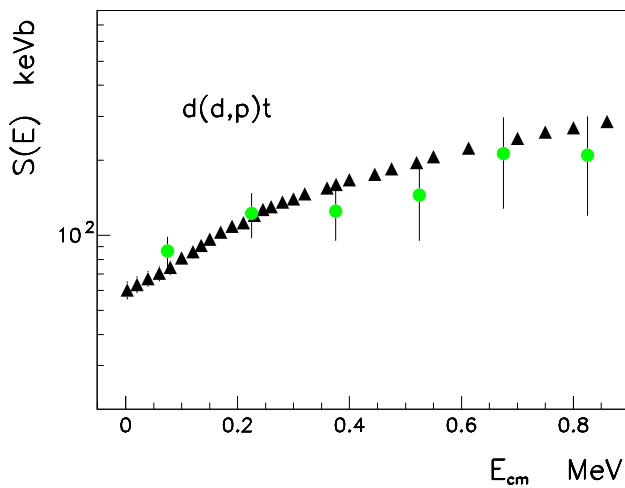


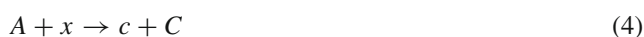
Fig. 6 TH $S(E)$ -factors for ${}^2\text{H}(d,p){}^3\text{H}$ reaction obtained using ${}^3\text{He}$ QF break-up (black triangles) and ${}^6\text{Li}$ QF break-up (green solid circles)

the pole invariance is verified. This is one of the most important validity test for THM, being the others the reproduction of direct data behaviour above the Coulomb barrier both for the excitation functions as well as the angular distributions.

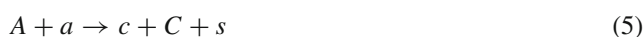
5 Inter-cluster momentum distribution and THM

The specific relevance of clusters and their dynamics is evident when one considers the role which is played in such a framework by the momentum distribution. In general principles THM can be discussed satisfactorily by considering the Plain Wave Impulse Approximation (PWIA); in this context one can factorize the binary reaction cross section of astrophysical interest in terms of the measured three-body one times the inter-cluster momentum distribution, $|\varphi(\mathbf{p}_s)|^2$ of the spectator inside the TH nucleus following the relation 3.

In such an approach, the Fourier transform of the bound-state wave function of the relative motion of the fragment s and particle x in the TH nucleus, $a = (sx)$, can be eliminated by a simple procedure allowing us to extract the half-off-energy-shell (HOES) binary reaction cross section (see Eq. (3)) which can be related with the on-energy-shell (OES) astrophysical factor. The usual aim for THM studies is to extract the cross section of an astrophysically relevant two-body reaction



from the quasi-free contribution to a selected three-body process,



with a the TH nucleus. Nevertheless, due to the presence of the other particles, the momentum distribution of the spec-

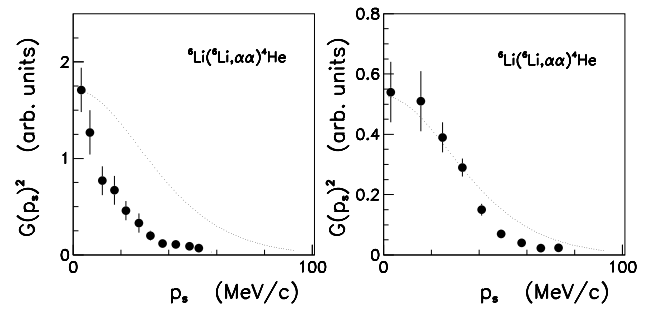


Fig. 7 Experimental momentum distribution for d inside ${}^6\text{Li}$ for the ${}^6\text{Li}({}^6\text{Li}, \alpha\alpha){}^4\text{He}$ reaction at 3.6 (panel a) and 5.9 MeV (panel b). Dashed line is the theoretical one discussed in [40]

tator s can be distorted thus having an impact on the final result.

This task was first fulfilled for the case of the α - d clusters in ${}^6\text{Li}$ in the pioneering work [44]. There it was shown for the α and d clusters constituting ${}^6\text{Li}$ that the experimental momentum distribution is distorted at lower transferred momenta, q_t . This is defined [40] as the transfer momentum from particle A to the system $B = c + C$ determined as the Galilean invariant transferred momentum

$$\mathbf{q}_t = \left(\frac{m_B}{m_A}\right)^{1/2} \mathbf{p}_A - \left(\frac{m_A}{m_B}\right)^{1/2} \mathbf{p}_B. \tag{6}$$

from the projectile A to the center-of-mass of the final system $B = C + c$.

Successively this behaviour was confirmed [41] after re-analyzing previous data from different experiments and comparing our results with others present in literature. This study helped to evaluate the dependence of the THM astrophysical factor on the full-width at half maximum momentum distribution (FWHM), which might introduce additional uncertainties to results extracted via this method. In [41] it was shown that errors introduced in the THM due to the momentum distribution uncertainties are much smaller (around 5%) than experimental errors caused by other sources for the ${}^6\text{Li}(d,\alpha){}^4\text{He}$ case.

In Fig. 7 the experimentally obtained intercluster momentum distribution for α - d clusters in ${}^6\text{Li}$ is obtained. On the left panel the case of the $({}^6\text{Li}, \alpha\alpha){}^4\text{He}$ at $E_{Li} = 3.6$ MeV (corresponding to a transferred momentum $q_t = 240$ MeV/c) is reported in comparison with the theoretical prediction for the momentum distribution reported in [41]. The distribution is clearly distorted, with a FWHM corresponding to 40 MeV/c. In the right panel a less distorted momentum distribution is reported, which corresponds to $E_{Li} = 5.9$ MeV. In this latter case the FWHM is 60 MeV/c which is still far from the un-distorted width of 73 MeV/c. This overall behaviour was explored, as stated before, in the eighties in the paper of [44]. Further studies and extension for ${}^6\text{Li}$ were provided in [40, 41].

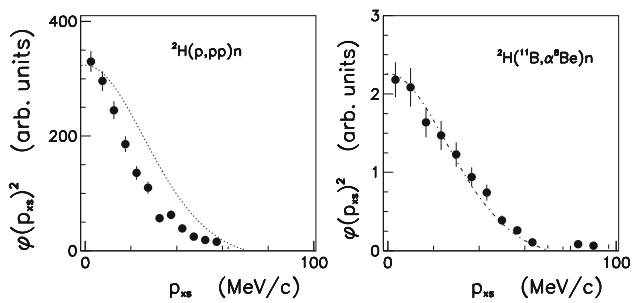


Fig. 8 Experimental momentum distribution for the proton inside deuteron derived according to the method explained in the text for the ${}^2\text{H}(p, pp)n$, (panel a), and ${}^2\text{H}({}^{11}\text{B}, \alpha{}^8\text{Be})n$, (panel b), reactions. The squared Hulthén function in momentum space is superimposed to data

The same behaviour discussed above for ${}^6\text{Li}$ was also highlighted for the other TH nuclei of interest for THM i.e. ${}^2\text{H}$, ${}^3\text{He}$ and ${}^9\text{Be}$. Among all other TH nuclei the simplest and by far most used one is deuterium. Among the advantages of using it is its relative low binding energy, the well known structure and momentum distribution and its availability as a cheap solid target in the form of enriched polyethylene foils (98% purity). Therefore deuterium was used in a huge series of THM experiments and its inter-cluster momentum distribution has been studied extensively for a big range of transferred momentum.

Two typical momentum distributions are plotted in Fig. 8. In particular in the left panel data from ${}^2\text{H}(p, pp)n$ reaction are reported which corresponds to a transferred momentum of 51 MeV/c (see Ref. [45] for details) together with the squared Hulthén function. A clear distortion is evident with the FWHM reduced to a value of 46 MeV/c. In the right panel data from the ${}^2\text{H}({}^{11}\text{B}, \alpha{}^8\text{Be})n$ process are reported (see reference [46, 47] for experimental details). It can be seen that in this case, where q_t is 210 MeV/c (thus significantly larger than the previous case), no distortion shows up and the width of the momentum distribution is equivalent to what is expected from the Hulthén function (58 MeV/c).

The third historically more used TH nucleus is ${}^3\text{He}$ which can be described in terms of $p \oplus d$ constituting clusters. Despite its rather high binding energy it has proved as a valuable nucleus for THM applications (see Refs. [19, 30, 31] and references therein). In figure 9 the inter-cluster momentum distribution is reported for ${}^3\text{He}$ for the cases of a low and high transferred momentum. Clearly in the left panel, showing the momentum distribution of p in ${}^3\text{He}$ for $q_t=120$ MeV/c, distortion effect dominates thus narrowing the width of the impulse distribution. On the right panel, however, data from the ${}^3\text{He}(p, pd)\text{H}$ at 100 MeV beam energy (corresponding to $q_t=375$ MeV/c) show a very small distortion from the theoretical prediction discussed in [40].

Another possible nucleus which may be treated as a potential TH is ${}^9\text{Be}$, which has a defined structure in terms of

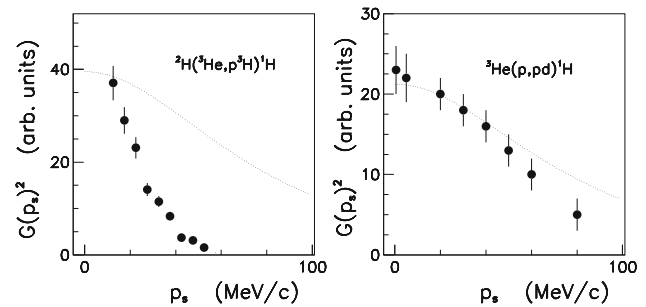


Fig. 9 Experimental momentum distribution for p in ${}^3\text{He}$ for the ${}^2\text{H}({}^3\text{He}, p{}^3\text{He})n$ reaction at 17 MeV (panel a) and the ${}^3\text{He}(p, pd)\text{H}$ at 100 MeV (panel b). Line is the theoretical prediction discussed in [40]

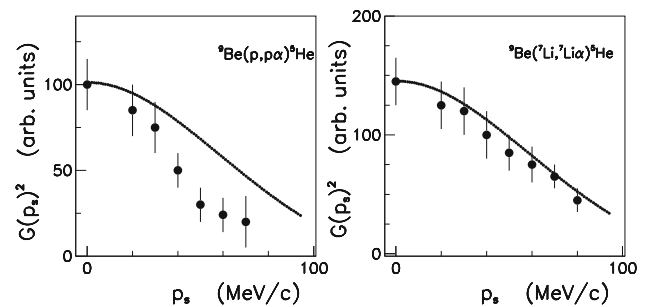


Fig. 10 Experimental momentum distribution for ${}^4\text{He}$ in ${}^9\text{Be}$ for the ${}^9\text{Be}(p, p\alpha){}^5\text{He}$ reaction at 47 MeV (a) and the ${}^9\text{Be}({}^7\text{Li}, {}^7\text{Li}\alpha){}^5\text{He}$ at 52 MeV (b). The solid line is the theoretical prediction as discussed in [40]

$\alpha \oplus {}^5\text{He}$. It was suggested in [20] its use as a potential source of exotic ${}^5\text{He}$ “virtual” beam. In Fig. 10 the ${}^9\text{Be}$ momentum distribution is reported for two different experimental cases. In the left panel the inter-cluster momentum distribution for the ${}^4\text{He}$ in ${}^9\text{Be}$ for the ${}^9\text{Be}(p, p\alpha){}^5\text{He}$ reaction at 47 MeV (corresponding to a $q_t=470$ MeV/c) is reported. A distortion with respect to the theoretical prediction (solid line) is apparent, coherently with the other examined nuclides. At higher transferred momenta, see right panel of picture 10 which represents the ${}^9\text{Be}({}^7\text{Li}, {}^7\text{Li}\alpha){}^5\text{He}$ at 52 MeV ($q_t=650$ MeV/c), the distortion disappears and the predicted theoretical trend fits the experimental data well.

From all those cases the role of the inter-cluster motion in THM is evident as well as the distortion of its momentum distribution for smaller transferred momenta.

Recently, ${}^{14}\text{N}$ was added to the list of TH nuclei with its ${}^{12}\text{C}+d$ configuration and used to measure the ${}^{12}\text{C}+{}^{12}\text{C}$ fusion at astrophysical energies [16]. This choice was inspired by previous works [48, 49] where a strong transfer component was found in the ${}^{14}\text{N}+{}^{12}\text{C}$ interaction at beam energies of 29 MeV and up. The PWIA theoretical behavior of the deuteron momentum distribution in terms of the squared Fourier transform of the radial wave function for the ${}^{12}\text{C}+d$ inter-cluster motion was obtained from a Woods–Saxon ${}^{12}\text{C}-d$ bound state potential. The standard geometrical parameters $r_0 = 1.25$ fm,

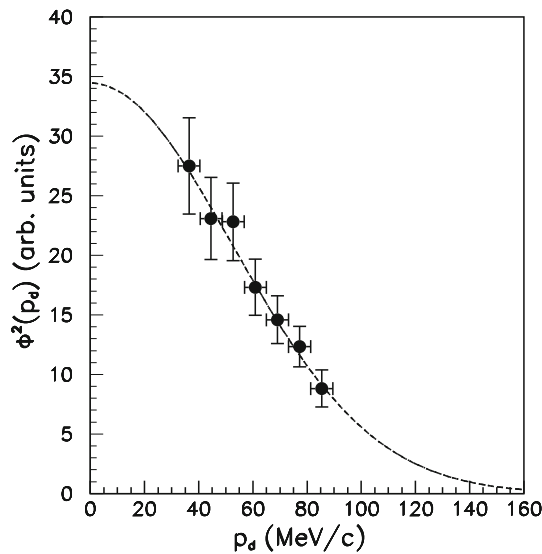


Fig. 11 Experimental momentum distribution for deuteron in ^{14}N for the $^{12}\text{C}(^{14}\text{N}, ^{20}\text{Ne}\alpha)^2\text{H}$ reaction at 30 MeV. The dashed line is the theoretical shape (see text for details)

$a = 0.65$ fm and $V_0 = 54.428$ MeV were adjusted to give the experimental ground state $^{12}\text{C}_{gs}$ -d binding energy in ^{14}N . The experimental shape of the momentum distribution was determined from $^{14}\text{N}+^{12}\text{C}$ measurement at 30 MeV of beam energy after selecting the $^{20}\text{Ne}+\alpha_{0,1}+d$ and $^{23}\text{Na}+p_{0,1}+d$ reaction channels (see [16] for details). The standard procedure on coincidence data, already discussed for the other cases, was applied over a restricted range of E_{cm} and θ_{cm} of less than 30 keV and 5° , respectively. A deuteron momentum distribution showing the largest range in momentum of the deuteron, p_d , covered in the experiment is reported in Fig. 11 as black filled circles. Error bars include statistical errors only. The dashed black line in the figure represents the theoretical shape normalized to the experimental data.

The p_d experimental upper limit of about 80 MeV/c is much less than 181 MeV/c, corresponding to the value of the on-the-energy-shell bound state wave number for the ^{12}C -d. This is the condition for the quasi-free mechanism to be dominant for example, for the HOES cross-section to be similar in shape to the on-energy-shell cross-section minimizing distortions [50,51]. Additional general details on the on-the-energy-shell bound state wave number and applicability of the pole approximation are given in the next section. Further work has been done to test the validity of the PWIA for this measurement. In particular it was proved that in the populated p_d experimental range there is agreement between the PWIA and DWBA theoretical shapes of the momentum distribution. This result will be presented in a forthcoming paper.

5.1 Influence of the deuteron d-state component in THM studies

As mentioned above, the effect of distortions has been addressed in the case of the p-n momentum distribution inside deuteron, corroborating the PWIA approach. A further source of systematic uncertainty is the use of approximate momentum distributions, i.e., the Fourier transform of the asymptotic radial wave function, and the neglect of the deuteron d-wave component. In [52], we report on the influence of the d-state contribution in describing the deuteron momentum distribution and its influence on TH experimental data. This is a crucial point in the extraction of the THM cross section, as uncertainty introduced by the momentum distribution description has to be taken into account. The s-state wave function can be given by the Hulthén wave function

$$u(r) = N(e^{-\alpha r} - e^{-\beta r}), \beta \gg \alpha. \tag{7}$$

In Eq. 7, $e^{-\alpha r}$ describes the asymptotic form of the Hulthén wave function while $e^{-\beta r}$ gives its modification at small distances in order to obtain $u(r) \sim r$ and $u(r_{r=0})=0$ [53–57]. The α parameter is defined as

$$\alpha = \frac{\sqrt{\epsilon_d m}}{\hbar} \tag{8}$$

where ϵ_d is the deuteron binding energy, m the nucleon mass and $N = \sqrt{\frac{2\alpha\beta(\alpha+\beta)}{(\alpha-\beta)^2}}$. If $\epsilon_d=2.2245$ MeV [56], one obtains $\alpha \approx 0.2316$ fm $^{-1}$ corresponding to a deuteron radius of ~ 4.32 fm [57]. The other quantities, β and the normalization constant N , have the values [55]

$$\beta \approx 5.98\alpha \tag{9}$$

$$N^2 = 0.780\text{fm}^{-1} \tag{10}$$

In order to take into account also the d-state component in the deuteron ground state wave function, it is possible to use the approximation of [55]

$$w(r) = \eta N(1 - e^{-\tau r})^5 e^{-\alpha r} \left(1 + \frac{3}{\alpha r} + \frac{3}{(\alpha r)^2}\right) \tag{11}$$

where $\tau=0.83$ fm $^{-1}$ and $\eta=0.029$. In [55], the authors evaluated a 4% d-state component over the whole deuteron ground-state wave function. The total deuteron wave function satisfies then the normalization condition

$$\int_0^\infty [u^2(r) + w^2(r)]dr = 1 \tag{12}$$

The behaviour of the s-state and d-state components is shown in Fig. 12, where the s-wave (described by the relation Eq. 7) is shown as dashed-black line while the d-wave (described by the relation Eq. 11) is reported as dot-dashed red line.

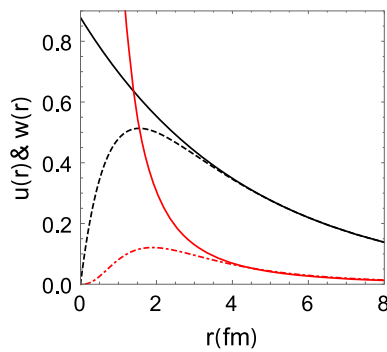


Fig. 12 The behaviour of exact *s* component of the deuteron wave function (Eq. 7) is shown as dashed black line, while the red dot-dashed line refers to the exact *d* component of Eq. 11. Full lines give the trend of the asymptotic forms, the colors maintaining the same meaning as above. Figure adapted from [52]

At large interaction radii *r*, the two functions describing the *s* and *d* states can be expressed in the simpler form

$$u(r)_{r \rightarrow \infty} \rightarrow A_s e^{-\alpha r} \tag{13}$$

$$w(r)_{r \rightarrow \infty} \rightarrow A_d e^{-\alpha r} \left(1 + \frac{3}{\alpha r} + \frac{3}{(\alpha r)^2} \right) \tag{14}$$

where the simplicity of the form of the wave function is connected with a weaker sensitivity of the tail of the wave function on the shape of the nuclear potential. Here, *A_s* and *A_d* are the asymptotic normalization constants for, respectively, *s* and *d* waves [56]. The behaviour of the asymptotic form for deuteron waves are shown as full-lines in Fig. 12, black and red for *s* and *d* state, respectively. It is clear that at large radii (*r* > 4 fm), the asymptotic forms given above coincides with the one given by Eq. 7 and Eq. 11.

In the case of TH applications, the available experimental data are usually taken in a very narrow range of momentum values, corresponding to the region where the QF mechanism is expected to be dominant.

Indeed, the applicability of the pole approximation is limited to small momenta *p_{xs}* given, for the break-up of a target in an *s*-wave cluster configuration, by [50,58,59]:

$$0 \leq p_{xs} \leq \kappa_{xs} \tag{15}$$

with *p_{xs}* the half-off energy shell (HOES) momentum of the cluster *x* when it interacts with the particle *a*, and *κ_{xs}* defined by $\kappa_{xs} = \sqrt{2\mu_{xs} B_{xs}}$, being *μ_{xs}* the *x* – *s* reduced mass. In the case of deuteron, such momentum range is $0 \leq p_{xs} \leq 40$ MeV/c, the upper limit corresponding to a minimum radius of about ~4 fm. At such radius, the exact and the asymptotic form of the *s*-component coincide within <1% while the for the *d*-component they coincide within ~4%, as shown Fig. 12.

By then considering the asymptotic behaviour of the momentum distribution, it is possible to evaluate the *d*-state contribution on the momentum distribution. Following the

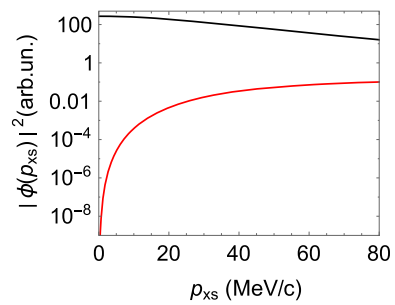


Fig. 13 Contributions of the *s*-wave (black line) and of the *d*-wave (red line) in momentum space deduced by means of the asymptotic behaviour. The semi-log scale allows one to estimate the contribution of the *d*-state component, i.e. lower than ~0.04%. Figure adapted from [52]

results of [52] such a result is displayed in Fig. 13, from which a contribution lower than ~0.04% is evident.

To account for the influence of the deuteron *d*-state component, two different THM study-cases were selected, namely the ¹¹B(*p,α*)⁸Be and ¹⁸O(*p,α*)¹⁵N reactions discussed in [47,60], respectively.

The effect of the *d*-state component of the deuteron wave function on the TH ¹¹B(*p,α*)⁸Be data has been also evaluated. In particular, the complete form of the deuteron wave function, including the *d*-state contribution, has been introduced in the same data discussed in [47]. The result in Fig. 14 shows the discrepancy ϵ

$$\epsilon = \frac{S'(E) - S(E)}{S(E)} \tag{16}$$

between the *S*(*E*)-factor extracted in [47], namely *S*, and the one extracted including the *d*-state component in the description of the ground state deuteron wave function, namely *S'*. The zero-energy *S*(*E*)-factor has a variation of ~0.4%, well below the quoted uncertainty of ~20% given in [47].

A further evaluation of the *d*-state influence on TH data has been performed for the ¹⁸O(*p,α*)¹⁵N reaction, studied via the application of the TH to the ²H(¹⁸O,*α* ¹⁵N)*n* QF reaction [60]. In particular, the same TH data discussed in [60] have been evaluated by introducing the *d*-wave component in the extraction of the resonance strength $\omega\gamma$ for the three ¹⁹F resonant levels contributing at 0.020 MeV, 0.090 MeV and 0.144 MeV in the ¹⁸O(*p,α*)¹⁵N center-of-mass energy [60]. In this case we defined the discrepancy ϵ as

$$\epsilon = \frac{\omega\gamma' - \omega\gamma}{\omega\gamma} \tag{17}$$

where the primed quantity represents the result obtained once the *d*-state component is taken into account. The results, displayed in Fig. 15, show a variation of less than ~0.1% for the 0.020 MeV resonance and less than ~0.05% for the 0.090 MeV resonance, respectively. In both case, as throughly dis-

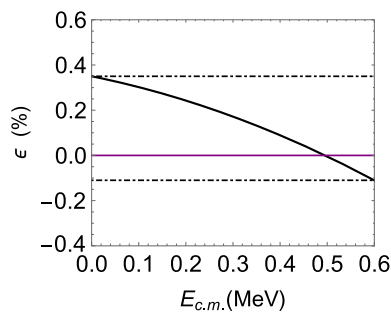


Fig. 14 The discrepancy ϵ of Eq. 16 (black line) for the $^{11}\text{B}(p,\alpha)^8\text{Be}$ case as function of the center-of-mass energy $E_{c.m.}$. The black dot-dashed lines set the higher and lower value of ϵ . Figure adapted from [52]

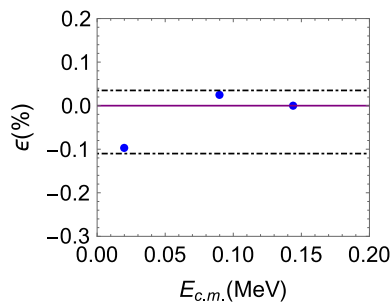


Fig. 15 The discrepancy ϵ of Eq. 17 is shown for the resonant 0.02 MeV, 0.09 MeV and 0.144 MeV levels (blue points) intervening in the $^{18}\text{O}(p,\alpha)^{15}\text{N}$ case. The black dot-dashed lines set the higher and lower value of ϵ . Figure adapted from [52]

cussed in [60], the 0.144 MeV level has been used for normalization, thus $\epsilon=0$ in this case.

5.2 Dependence of THM result on the momentum distribution width

As it can be seen from Eq. 3 the extraction of the binary reaction of astrophysical interest cross section depends also on the momentum distribution, and in particular on its width. This holds for all the TH nuclei discussed above but it was quantitatively determined for ^6Li . As extensively reported in [41], such an impact, though being a minor contribution to uncertainties with respect to other sources (e.g. experimental errors) has a not-negligible impact. In Fig. 16 the $S(E)$ -factor for the $^6\text{Li}(d,\alpha)^4\text{He}$ reaction is plotted. The solid line represents the value extracted from formula (Eq. 3) after assuming an un-distorted momentum distribution (i.e. ~ 70 MeV/c wide). The dashed line is for a distorted width of 61 MeV/c, and the dotted line represents the more distorted case of 50 MeV/c width. As it is possible to see variations up to 15% arise if the more distorted distribution is used in place of the un-distorted one. In the case reported in the figure, the THM measurement of $^6\text{Li}(d,\alpha)^4\text{He}$ after applying the method to QF break-up of the $^6\text{Li}(^6\text{Li},\alpha)^4\text{He}$ process induced at a

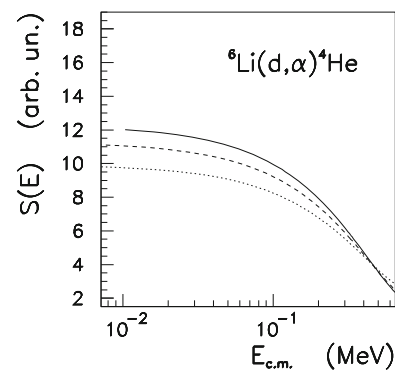


Fig. 16 Experimental $^6\text{Li}(d,\alpha)^4\text{He}$ $S(E)$ factor, extracted via the THM, for different choices of the α momentum distribution width inside ^6Li . The solid line represents the case of a momentum distribution 70 MeV/c wide, the dashed line is for a width of 61 MeV/c, and dotted line is for 50 MeV/c, as it is reported in [41]

beam energy of 5.9 MeV (corresponding to $q_t=270$ MeV/c with a distribution 61 MeV/c wide) we can estimate uncertainties arising from distortions to account for 6% errors (to be compared with 15% of the combined systematic and statistical errors). Similar results are obtained for other THM applications.

Therefore in all the case of THM applications available in literature Eq. 3 is applied using as the momentum distribution width the one which is measured in the same experiment. In this way, the eventual distortions which may be present in the case of low q_t can be taken into account in the binary cross section extraction.

6 Future THM nuclei for next generation experiments

The gravitational wave signal GW170817 attributed to the merger of two neutron stars has ushered us into a new era of nuclear astrophysics. The concurrent observation of the GW170817 and of the astronomical transient in the galaxy NGC 4993 by numerous telescopes, from radio to X-ray wavelengths, made it possible to identify a realistic site for the r-process [61], producing about half of the elements heavier than iron. Observations showed the production of neutron-rich material, as found in the debris from a neutron-star merger (see, for instance, [62] and references therein).

Such turning point in nuclear astrophysics requires further investigations of nuclear reactions involved in the study of the r-process. Besides the reactions directly involved in the r-process, essentially n-captures on unstable nuclei that can be studied using deuterons as sources of virtual neutrons, as already done for $^6\text{Li}+n$, $^{10}\text{B}+n$ and $^{17}\text{O}+n$ reactions, two kinds of reactions are especially important. These include reactions involving heavy ions, such as the $^{12}\text{C}+^{12}\text{C}$ and the $^{16}\text{O}+^{16}\text{O}$ fusion reactions, which influence the late evolu-

tion of massive stars, eventually forming a neutron star or a black hole depending, among others, on their residual masses [63]. On the other hand, a number of alpha-induced reaction on neutron rich nuclei may play an important role in core-collapse supernovae (the so-called *alpha*-process [64]), at energies not exceeding few MeV.

Therefore, two challenges affect the investigations of reactions of interest for the investigation of the r-process and the physics behind multimessenger astronomy. First, the need of nuclei whose ground states are clusterized and can be described as a heavy ion, such as carbon or oxygen, plus a cluster which would act as a spectator to the $^{12}\text{C}+^{12}\text{C}$ and the $^{16}\text{O}+^{16}\text{O}$ fusion. Such problem is not trivial; an example is given the study of $^{12}\text{C}+^{12}\text{C}$ fusion. While the use of ^{14}N to transfer a ^{12}C nucleus and induced $^{12}\text{C}+^{12}\text{C}$ fusion turned out to be very successful [16], the use of ^{16}O did not make it possible to populated the energy region of astrophysical energy, around 2 MeV in the $^{12}\text{C}+^{12}\text{C}$ center-of-mass system, in QF kinematics [65].

A similar discussion applies to understanding the $^{16}\text{O}+^{16}\text{O}$ fusion [66]. While ^{20}Ne would be a very useful THM nucleus, making it possible to apply the THM technique through the use of active targets (such as TEXAT [67]), ^{20}Ne ground state is deformed, making the application of THM more complicated and, still, under development [68]. Such isotope would be an interesting TH nucleus also for the possibility to transfer alpha particles and investigate α -induced reaction under conditions easier to reach for present-day RIB facilities.

Indeed, while ^6Li has been routinely used as a virtual source of deuterons and alpha particles, as discussed at length in previous sections, its low binding energy of about 1.47 MeV makes it generally unsuited for applications with radioactive ion beams. Since the beam energies supplied by most RIB facilities are above 10 MeV, in most cases it is not possible to reach astrophysical energies using ^6Li to transfer an alpha particle, right because of its low binding energy. Even the $d - \alpha$ intercluster motion is enough to compensate for the beam energies. Therefore, ^{20}Ne may represent an alternative source of virtual alpha particles to investigate α -induced reactions, especially in the case RIBs are involved. An alternative candidate may ^{18}O , for which the α channel is the dominant charge transfer mode [69], but cannot be profitably used in active targets. On the other hand, the high binding energy of $^{14}\text{C}+\alpha$ in ^{18}O , 6.228 MeV, quite higher than the one for $^{16}\text{O}+\alpha$ in ^{20}Ne (4.729 MeV), would make ^{18}O especially suitable for THM studies involving RIBs. Studies are ongoing to assess the possibility to use such systems as future THM nuclei for next generation experiments.

Acknowledgements The author acknowledge “Programma ricerca di ateneo UNICT 2020-22 linea2” and “Starting grant 2020” of University of Catania. C.A.B. acknowledges support by the U.S. DOE grant DE-FG02-08ER41533 and by funding contributed through the LANL

Collaborative Research Program by the Texas A&M System National Laboratory Office and Los Alamos National Laboratory.

Data Availability Statement This manuscript has no associated data or the data will not be deposited. [Authors’ comment: Data are deposited in INFN-LNS data repository. Researchers who want to access data are kindly asked to contact the authors.]

References

- G. Baur, C.A. Bertulani, H. Rebel, Nucl. Phys. A **458**, 188 (1986)
- C. Spitaleri 1991, in *Problems of Fundamental Modern Physics, II*, eds. by R. Cherubini, P. Dalpiaz, B. Minetti Proceedings (World Scientific Publishing, Singapore, 1991), p. 21
- M.L. Sergi, C. Spitaleri, M. La Cognata et al., Phys. Rev. C **91**, 065803 (2015)
- R.G. Pizzone, G. D’Agata, C. Spitaleri et al., ApJ. **836**, 57 (2017)
- I. Indelicato, M. La Cognata et al., Astrophys. J. **845**, 19 (2017)
- G. D’Agata, R.G. Pizzone et al., Astrophys. J. **860**, 61 (2018)
- R.G. Pizzone, C. Spampinato et al., Eur. Phys. J. A **56**, 199 (2020)
- M. Gulino et al., Phys. Rec. **C87**, 012801 (2013)
- G.L. Guardo, C. Spitaleri, L. Lamia et al., Phys. Rev. C **95**, 025807 (2017)
- G.L. Guardo, C. Spitaleri, L. Lamia et al., Eur. Phys. J. A **55**, 211 (2019)
- S. Cherubini et al., Phys. Rev. C **92**, 015805 (2015)
- R.G. Pizzone, B. Roeder, M. Mckluskey et al., Eur. Phys. J. A **52**, 24 (2016)
- M. La Cognata, R.G. Pizzone et al., Ap. J. **846**, 65 (2017)
- L. Lamia et al., ApJ. **850**, 175 (2017)
- L. Lamia, M. Mazzocco, R.G. Pizzone et al., Astrophys. J. **879**, 23 (2019)
- A. Tumino, C. Spitaleri, M. La Cognata et al., Nature **557**, 687–690 (2018)
- M. Lattuada et al., ApJ. **562**, 1076 (2001)
- C. Spitaleri et al., Phys. Rev. C **63**, 055801 (2001)
- R.G. Pizzone, L. Lamia, C. Spitaleri et al., Phys. Rev. C **83**, 045801 (2011)
- C. Spitaleri et al., Eur. Phys. J. A **56**, 18 (2020)
- S.T. Butler, Phys. Rev. **80**, 1095 (1950)
- S.T. Butler, Nature **166**, 709 (1950)
- S.T. Butler, Proc. R. Soc. A **208**, 559 (1951)
- C. Spitaleri et al., Nucl. Phys. A **719**, 99c (2003)
- R.E. Tribble et al., Rep. Prog. Phys. **77**, 10690 (2014)
- C. Spitaleri, M. La Cognata, L. Lamia, A.M. Mukhamedzhanov, R.G. Pizzone, Eur. Phys. J. A **52**, 77 (2016)
- C. Spitaleri, M. La Cognata, L. Lamia, R.G. Pizzone, A. Tumino, Eur. Phys. J. A **55**, 161 (2019)
- M. La Cognata et al., Phys. Rev. Lett. **101**, 152501 (2008)
- C.A. Bertulani, A. Gade, Phys. Rep. **485**, 195 (2010)
- A. Tumino et al., Eur. Phys. J. A **25**, 649 (2005)
- R.G. Pizzone, C. Spitaleri, C. Bertulani et al., Phys. Rev. C **87**, 025805 (2013)
- R.G. Pizzone, R. Sparta, C. Bertulani et al., ApJ. **786**, 112 (2014)
- R.G. Pizzone et al., A. & A. **398**, 423 (2003)
- C. Spitaleri, L. Lamia et al., Phys. Rev. C **90**, 035801 (2014)
- L. Lamia, C. Spitaleri, E. Tognelli et al., Astrophys. J. **811**, 99 (2015)
- M. Zadro et al., Phys. Rev. C **40**, 181 (1989)
- M. Aliotta, C. Spitaleri et al., Eur. Phys. J. **9**, 435 (2000)
- A. Rinollo et al., Nucl. Phys. A **758**, 146c (2003)
- A. Tumino et al., Phys. Lett. B **705**, 546 (2011)
- R.G. Pizzone et al., Phys. Rev. C **80**, 025807 (2009)

41. R.G. Pizzone, C. Spitaleri, S. Cherubini et al., *Phys. Rev. C* **71**, 058801 (2005)
42. A. Krauss et al., *Nucl. Phys. A* **465** (1987)
43. R.E. Brown, N. Jarmie, *Phys. Rev. C* **41**, 1391 (1990)
44. S. Barbarino, M. Lattuada, F. Riggi, C. Spitaleri, D. Vinciguerra, *Phys. Rev. C* **21**, 1104 (1980)
45. A. Tumino et al., *Phys. Rev. Lett.* **98**, 252502 (2007)
46. L. Lamia et al., *Nuovo Cimento C* **31**, 423–431 (2008)
47. L. Lamia et al., *J. Phys. G* **39**, 015106 (2012)
48. R.W. Zurmühle et al., *Phys. Rev. C* **49**, 2549 (1994)
49. T.L. Belyaeva, N.S. Zelenskaya, *Phys. Rev. C* **66**, 034604 (2002)
50. I.S. Shapiro, *Nucl. Phys.* **61**, 353 (1968)
51. E.I. Dolinsky, P.O. Dzhamalov, A.M. Mukhamedzhanov, *Nucl. Phys. A* **202**, 97 (1973)
52. L. Lamia et al., *Phys. Rev. C* **85**, 025805 (2012)
53. A.S. Davydov, *Teoria del Nucleo Atomico*, Zanichelli Bologna (1966)
54. E. Segré, *Nuclei and Particles* (Benjamin-Cummings Pub Co, Menlo Park, 1977)
55. R.J. Adler et al., *Phys. Rev. C* **16**, 3 (1977)
56. V.A. Babenko, *Phys. At. Nuclei* **74**, 352–357 (2011)
57. R. Evans, *The Atomic Nucleus* (McGraw-Hill, New York, 1969)
58. I.S. Shapir, in *Interaction of High-Energy Particles and Nuclei. International School of Physics Enrico Fermi, Course 38* (Academic Press, New York, 1967), p. 210
59. I.S. Shapiro, *Sov. Phys. Uspekhi* **10**, 515 (1968)
60. M. La Cognata et al., *Astron. Phys. J.* **708**, 796 (2010)
61. M.R. Mumpowe et al., *Prog. Part. Nucl. Phys.* **86**, 86 (2016)
62. D. Watson et al., *Nature* **574**, 497 (2019)
63. A. Chieffi, M. Limongi, *Astrophys. J.* **764**, 21 (2013)
64. T. Sasaqui et al., *Astrophys. J.* **634**, 1173 (2005)
65. G.G. Rapisarda et al., *J. Phys. Conf. Ser.* **703**, 012024 (2016)
66. S. Hayakawa et al., *EPJ Web Conf.* **117**, 09013 (2016)
67. E. Koshchiy et al., *Nucl. Instrum. Methods Phys. Res. A* **957**, 21 (2020)
68. S. Typel, private communication
69. D.C. Rafferty et al., *Phys. Rev. C* **94**, 024607 (2016)